Annals of Botany **122**: 359–371, 2018
doi: 10.1093/aob/mcy075, available online at www.academic.oup.com/aob

ANNALS OF BOTANY
Founded 1887

A *Pelota-like* gene regulates root development and defence responses in rice

Wona Ding[1], Jing Wu[2], Jin Ye[2], Wenjuan Zheng[1], Shanshan Wang[2], Xinni Zhu[2], Jiaqin Zhou[1], Zhichong Pan[1], Botao Zhang[3,*] and Shihua Zhu[1,*]

[1]College of Science & Technology, Ningbo University, Ningbo 315211, PR China, [2]School of Marine Sciences, Ningbo University, Ningbo 315211, PR China and [3]Cixi Institute of Biomedical Engineering, Ningbo Institute of Materials Technology and Engineering, Chinese Academy of Sciences, Ningbo 315201, PR China
**For correspondence. E-mail zhangbotao@nimte.ac.cn or zhushihua@nbu.edu.cn*

Received: 23 November 2017 Returned for revision: 14 March 2018 Editorial decision: 13 April 2018 Accepted: 19 April 2018
Published electronically 16 May 2018

• **Background and Aims** *Pelota* (*Pelo*) are evolutionarily conserved genes reported to be involved in ribosome rescue, cell cycle control and meiotic cell division. However, there is little known about their function in plants. The aim of this study was to elucidate the function of an ethylmethane sulphonate (EMS)-derived mutation of a *Pelo-like* gene in rice (named *Ospelo*).
• **Methods** A dysfunctional mutant was used to characterize the function of *OsPelo*. Analyses of its expression and sub-cellular localization were performed. The whole-genome transcriptomic change in leaves of *Ospelo* was also investigated by RNA sequencing.
• **Key Results** The *Ospelo* mutant showed defects in root system development and spotted leaves at early seedling stages. Map-based cloning revealed that the mutation occurred in the putative *Pelo* gene. *OsPelo* was found to be expressed in various tissues throughout the plant, and the protein was located in mitochondria. Defence responses were induced in the *Ospelo* mutant, as shown by enhanced resistance to the bacterial pathogen *Xanthomonas oryzae* pv. *oryzae*, coupled with upregulation of three pathogenesis-related marker genes. In addition, whole-genome transcriptome analysis showed that *OsPelo* was significantly associated with a number of biological processes, including translation, metabolism and biotic stress response. Detailed analysis showed that activation of a number of innate immunity-related genes might be responsible for the enhanced disease resistance in the *Ospelo* mutant.
• **Conclusions** These results demonstrate that *OsPelo* positively regulates root development while its loss of function enhances pathogen resistance by pre-activation of defence responses in rice.

Key words: Short root, spotted-leaf mutant, defence responses, RNA-seq, *Oryza sativa.*

INTRODUCTION

Pelota (PELO) is an evolutionarily conserved protein and has been identified in a number of species, including *Drosophila* (Eberhart and Wasserman, 1995), archaebacteria (Ragan *et al.*, 1996), yeast (Davis and Engebrecht, 1998), *Arabidopsis thaliana* (Caryl *et al.*, 2000), human (Shamsadin *et al.*, 2000), mouse (Shamsadin *et al.*, 2002) and tomato (Lapidot *et al.*, 2015). The PELO proteins contain 347–395 amino acid residues and RNA-binding domains similar to that found in the family members of the eukaryotic release factor 1 (eRF1) family members, which play roles in termination of protein synthesis (Davis and Engebrecht, 1998).

The study in *Drosophila* first identified that the cell cycle is arrested during the meiotic G_2/M transition phase in germline cells of *Pelo* male homozygotes, while only mitotic division is affected during oogenesis (Eberhart and Wasserman, 1995). In addition, the eyes of *Pelo* homozygotes are smaller than those of their heterozygous siblings. Further study revealed a critical role for PELO proteins in regulating self-renewal of germline stem cells (GSCs) by repressing the differentiation pathway (Xi *et al.*, 2005). Disruption of the balance between self-renewal and differentiation of GSCs impaired the fertility of loss-of-function *pelo* mutant females. A similar role for PELO protein in meiotic and mitotic division was also found in *Saccharomyces cerevisiae*, where the disruption *Dom34*, the orthologue gene of *Pelo*, resulted in growth retardation and defective sporulation (Davis and Engebrecht, 1998). In mice, disruption of the *Pelo* gene caused early embryonic lethality and cell cycle defects (Adham *et al.*, 2003). Further analysis found that PELO mediated gonocyte maturation and maintenance of spermatogonial stem cells in mouse testes (Raju *et al.*, 2015). PELO is also found to regulate extraembryonic endoderm development and epidermal differentiation, and to inhibit tumour progression and invasion (Nyamsuren *et al.*, 2014; Pedersen *et al.*, 2014; Elkenani *et al.*, 2016). In addition, PELO is involved in high efficiency viral replication (Wu *et al.*, 2014), and regulates a resistance reaction to begomovirus in tomato (Lapidot *et al.*, 2015).

Extensive studies have been conducted in yeast to characterize the function of PELO at the molecular level. The PELO-coding orthologue *Dom34* together with its interacting partner *Hbs1* participate in an RNA quality control mechanism called no-go decay (NGD) for the recycling of stalled ribosomes (Doma and Parker, 2006; Shoemaker and Green, 2011; Guydosh and Green, 2014). The structure of the DOM34–HBS1 complex is similar to that

of eRF1 and eRF3, but *Dom34* does not have motifs for codon recognition and peptide release (Chen *et al.*, 2010; Becker *et al.*, 2011). It was proposed that the DOM34–HBS1 complex binds to the ribosomal A site to promote dissociation of ribosome subunits (Shoemaker *et al.*, 2010). In addition to the RNA quality control in the NGD pathway, DOM34–HBS1 is also important for non-stop decay (NSD), i.e. decay of non-functional 18S rRNAs and mRNAs with premature stop codons (Cole *et al.*, 2009; Tsuboi *et al.*, 2012; Saito *et al.*, 2013). The DOM34–HBS1 complex also mediates dissociation of inactive 80S ribosomes to promote the restart of translation after stress (van den Elzen *et al.*, 2014). The roles of DOM34/PELO in mRNA quality control are conserved in *Drosophila* and human (Ikeuchi *et al.*, 2016; Hashimoto *et al.*, 2017). The PELO–HBS1 complex is also involved in transposon silencing in the *Drosophila* germline (Yang *et al.*, 2015). Recently, studies showed that defects in *GTPBP2*, a PELO-binding partner in mammals, resulted in ribosome stalling in a $tRNA^{Arg}$ (*UCU*) mutant background and the death of mouse neurons (Ishimura *et al.*, 2014; Kirmizitas *et al.*, 2014).

Little is yet known about the overall function of *Pelo* genes in plants. In this study, a *Pelo*-deficient rice mutant was isolated from an ethylmethane sulphonate (EMS)-mutagenized library. We describe a root development defect, a spotted-leaf phenotype and enhanced pathogen resistance for *Pelo* null rice.

MATERIALS AND METHODS

Plant materials and growth conditions

The rice mutant *Ospelo* was isolated from an EMS-mutagenized rice (*Oryza sativa* L. *indica*, 'Kasalath') mutant library. Hydroponic experiments were conducted in normal rice culture solution with the pH adjusted to 5.5 (Zhu *et al.*, 2012). In all hydroponic experiments, plants were grown in a greenhouse with a 12 h light (30 °C)/12 h dark (22 °C) cycle (16 000 lux) and a humidity of 70 %.

Acetocarmine and 5-ethynyl-2'-deoxyuridine (EdU) staining

Primary root tips of 4-day-old wild type (WT) and *Ospelo* plants were stained with 1 % acetocarmine solution for 10 min. After washing with 45 % acetic acid solution, they were mounted on glass slides and examined with a stereo microscope (Leica MZ95). EdU staining was conducted using an EdU kit (C10350, Click-iT EdU Alexa Fluor 488 HCS assay; Invitrogen) according to the manufacturer's instruction. Roots of 4-day-old WT and *Ospelo* plants were immersed in 20 mM EdU solution for 2 h and then fixed for 30 min in 3.7 % formaldehyde solution in phosphate buffer (pH 7.2) with 0.1 % Triton X-100. After that they were incubated with EdU detection cocktail for 30 min and examined with the green fluorescent protein (GFP) channel on a confocal laser-scanning microscope (Zeiss LSM 510, Jena, Germany). More than ten root samples of each genotype were examined, and the experiment was repeated twice.

Trypan blue staining

Trypan blue staining was performed on fresh leaves as previously described (Yin *et al.*, 2000). In brief, leaf samples were submerged in lactic acid–phenol–trypan blue (LPTB) solution [2.5 mg mL^{-1} trypan blue, 25 % (w/v) lactic acid, 23 % water-saturated phenol and 25 % glycerol in H_2O] at 30 °C for 12 h. The LPTB solution was then replaced with a chloral hydrate solution (50 g in 20 mL of H_2O) for destaining. After multiple changes of chloral hydrate solution for 4 d, leaf samples were washed with H_2O and mounted on glass slides before being examined with a stereo microscope (Leica MZ95). More than ten leaf samples were examined for each genotype, and the experiment was repeated three times.

Pollen activity staining assay

Spikelets about to flower from the WT and *Ospelo* were chosen for examination. After carefully opening the hull, anthers were placed in several drops of 1 % I_2–KI solution on glass slides and crumbled to release pollens. Then they were examined with a light microscope (Nikon eclipse 80i). Samples from more than five plants of each genotype were examined, and the experiment was repeated twice.

Histological observation

Root tips from 4-day-old plants were fixed overnight at 4 °C in 2.5 % glutaraldehyde in 0.1 M sodium phosphate buffer, pH 7.2, and washed three times for 30 min in the same buffer. The samples were then refixed in OsO_4 for 4 h at room temperature and washed for 30 min in the same buffer. Samples were dehydrated in a gradient ethanol, embedded in pure Spurr resin and polymerized overnight at 70 °C. Semi-thin sections (2 μm thick) were made using diamond knives on a power Tome XL microtome (RMC-Boeckeler Instruments, Tucson, AZ, USA) and stained with 0.1 % methylene blue for 3–5 min at 70 °C. The samples were rinsed with distilled water and visualized with a microscope (Nikon 90i, Japan).

Mapping and cloning of OsPelo

A mapping population was generated from crosses between the homozygous *Ospelo* mutant and *japonica* variety Nipponbare. A total of 30 and 538 short root plants from the F_2 population were used for primary and fine mapping of *OsPelo*, respectively. The *OsPelo* gene was localized to a region of 411 kb between the sequence-tagged site (STS) markers STS1 and STS2 on chromosome 4. Primers used are listed in Supplementary Data Table S1. The *OsPelo* gene was selected from 52 putative protein-coding genes as one of the candidate genes. To identify the mutation site, genes were amplified by PCR from the genomic DNA of both WT and *Ospelo* plants and used for Sanger sequencing analysis.

Construction of vectors and plant transformation

The coding region of *OsPelo* was PCR amplified and put into the pUCM-T vector (Takara). After sequencing confirmation, the fragment was excised from the pUCM-T vector by *Bam*HI and *Pst*I digestion and ligated into the corresponding site of pCAMBIA1300. A 2264 bp promoter of *OsPelo* was

obtained by PCR and inserted into the *Hin*dIII/*Bam*HI site in front of the *OsPelo* coding region to drive its expression. The promoter was also put into the *Hin*dIII/*Bam*HI site of vector pCAMBIA1300NH-GUS to create a transcriptional fusion of the *OsPelo* promoter and the β-glucuronidase (GUS) coding sequence, *OsPelop::GUS*. The above constructs were used for *Agrobacterium tumefaciens*-mediated rice transformation of the WT or *Ospelo* as described (Chen *et al.*, 2003).

Histochemical analysis and GUS assay

Histochemical GUS staining was performed as previously described (Ding *et al.*, 2015). Transgenic plant samples and freehand cross-section samples were incubated with GUS staining solution (100 mmol L^{-1} NaH_2PO_4 buffer pH 7.0, 0.5 % Triton X-100, 0.5 mg mL^{-1} X-Gluc and 20 % methanol) overnight at 37 °C. Tissues were subsequently rinsed and mounted on slides, and photographed using a stereo microscope (Leica MZ95, Nussloch, Germany).

Sub-cellular localization of OsPELO

The full-length coding sequence of *OsPelo* with the eliminated stop codon was inserted in-frame before the coding sequence of a soluble modified GFP (smGFP4). The OsPELO–GFP fusion-coding sequence was subcloned into the binary vector 35S-pCAMBIA1301. The resulting construct was sequenced to verify in-frame fusion and used for transient transformation of onion epidermis using a biolistic PDS-1000/He particle delivery system (Bio-Rad, Hercules, CA, USA). Alternatice oxidase (AOX)–red fluorescent protein (RFP) located to the mitochondria was co-transformed as a mitochondrial marker. The GFP and RFP were visualized using a confocal laser-scanning microscope (Zeiss LSM 510). The experiment was repeated twice.

Determination of resistance to bacterial blight in Ospelo

Three races of *Xanthomonas oryzae* pv. *oryzae* (*Xoo*) were used for evaluation of bacterial blight resistance. The Philippines races PXO71, PXO99 and PXO145 were kindly provided by Dr Jie Zhou of the Institute of Virology and Biotechnology, Zhejiang Academy of Agricultural Sciences, China. New fully expanded leaves of ten independent WT and *Ospelo* plants at the maximum tillering stage were inoculated for each race of *Xoo* using the clipping leaf method (Kauffman *et al.*, 1973). The lesion length on inoculated plants was measured 3 weeks after inoculation.

Quantitative real-time PCR (qRT-PCR) analysis

RNA was extracted from three biological replicates of leaf samples of 20-day-old WT and *Ospelo* plants using RNAiso plus (Takara). Three technical replicates were performed for each sample. The first-strand cDNA was synthesized from total RNA using Superscript II (Invitrogen, Carlsbad, CA, USA) and used as the qRT-PCR template. Real-time PCR analysis was performed using a Roche Lightcycler480 real-time PCR system with SYBR Premix Ex Taq (Takara). Primers used are listed in Supplementary Data Table S1. The *Ubiquitin* gene (*LOC_Os03g13170*) in rice was used as a reference gene.

Transcriptome sequencing

Total RNA was extracted from leaves of 20-day-old WT and *Ospelo* plants under normal conditions using the RNeasy Plant Mini Kit (Qiagen, USA). Three biological replicates for each genotype were collected. RNA was quantified using the Nanodrop-2000 (ThermoFisher, USA) and RNA quality was then examined using a 2100 Bioanalyzer (Agilent Technologies, USA). High-quality RNA samples for library construction were selected based on the 260/280 nm ratio and RNA integrity number (RIN) above 2.0 and 7.0, respectively. Sequencing libraries were prepared using the TruSeq Stranded mRNA LTSample Prep Kit (Illumina, San Diego, CA, USA) according to the manufacturer's instructions. Libraries were subjected to 125 cycles of paired-end sequencing with the Illumina HiSeq2500 system according to the manufacturer's instructions. The raw sequencing data have been uploaded to the SRA (Sequence Read Archive; https://www.ncbi.nlm.nih.gov/sra) database (accession no. SRP117240).

Differentially expressed gene analysis

Raw reads were first processed using in-house Perl scripts. In this step, clean reads were obtained by removing reads containing adaptor, reads containing ploy-N and low-quality reads (the number of bases with quality value ≤20 is more than 35). The retained high-quality reads, i.e. clean reads, were then analysed by the TopHat–Cufflinks pipeline (Trapnell *et al.*, 2012). Briefly, clean reads were mapped to the rice genome (MSU version 7, http://rice.plantbiology.msu.edu/) using TopHat. Cufflinks was then used for transcriptome assembly and assessment of the FPKM (fragments per kilobase of transcript per million mapped reads) value. Counts of mapped reads to genes were obtained with HTSeq (http://www-huber.embl.de/users/anders/HTSeq/doc/overview.html) and differentially expressed genes (DEGs) were determined using DESeq2 (http://bioconductor.org/packages/release/bioc/html/DESeq2.html) by the Negative Binomial Distribution test (Love *et al.*, 2014; Anders *et al.*, 2015). Genes with a false discovery rate (FDR)-adjusted P-value <0.05 were assigned as DEGs. Gene Ontology (GO) annotation was conducted by querying Swiss-Prot (http://www.uniprot.org) with transcripts of DEGs and enrichment analysis was performed by the hypergeometric distribution test using R with a threshold FDR-adjusted P-value <0.01. The Kyoto Encyclopedia of Genes and Genomes (KEGG) pathway enrichment analysis was conducted by PlantGSEA with a threshold FDR-adjusted P-value <0.01 (Yi *et al.*, 2013). The functional categorization of DEGs was conducted by MapMan (Thimm *et al.*, 2004).

RESULTS

The rice Ospelo *mutant showed root and leaf growth defects*

A mutant showing short roots and spotted leaves was isolated from an EMS-mutagenized rice mutant library (*Oryza sativa* L. *indica* 'Kasalath'). The mutant was designated as *Ospelo*, which will be described later on (Fig. 1A). After growth in culture solution for 7 d, the primary root length of *Ospelo* (8.91 ± 1.06 cm) was only 57.9 % of that of the WT (15.38 ± 0.88 cm) (Fig. 1B). Moreover, the length of adventitious roots and lateral roots of *Ospelo* was also significantly shorter than that of those of the WT (Fig. 1B), while shoot height was slightly shorter than that of the WT (Fig. 1B).

To investigate the cause of the short root phenotype of *Ospelo* at a cellular level, root longitudinal section analysis was conducted. It showed that the radial organization

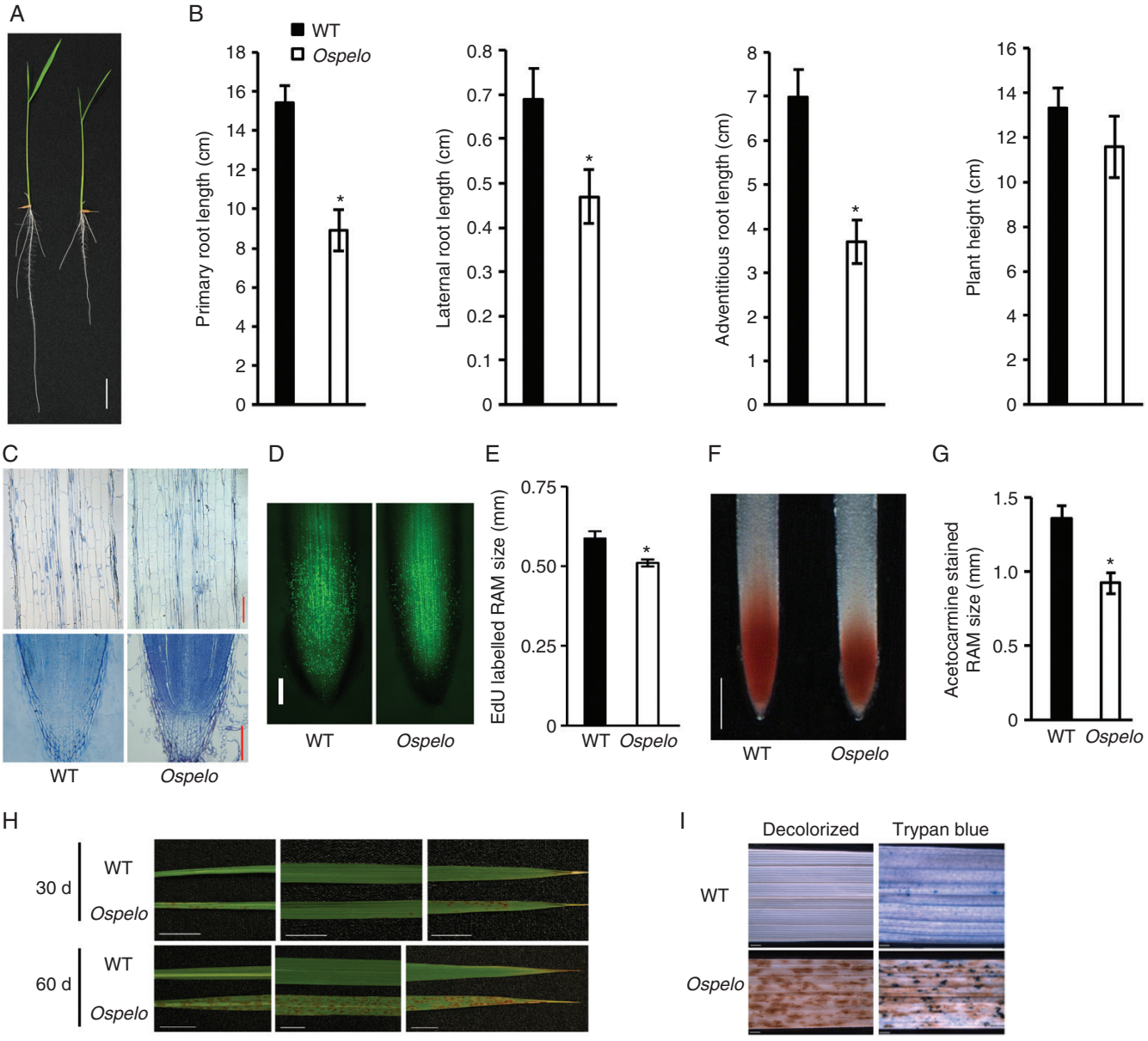

FIG. 1. Phenotypic characterization of *Ospelo*. (A) Growth phenotype of 7-day-old WT and *Ospelo* plants. Scale bar = 2 cm. (B) The primary, lateral and adventitious root length of the 7-day-old WT and *Ospelo* plants. The three longest adventitious roots and the 20 longest lateral roots on each primary root were counted. Error bars represent the s.d. (n = 20). (C) Longitudinal sections of the maturation zone (top) and root tip (bottom) of 4-day-old WT and *Ospelo* plants. Scale bars = 100 µm. (D) S-phase entry of 4-day-old WT and *Ospelo* root tips visualized by EdU staining. Scale bar = 100 µm. (E) Size of EdU-labelled root apical meristems (RAMs) of 4-day-old WT and *Ospelo* plants. Error bars represent the s.d. (n = 10). (F) Acetocarmine staining of root tips of 4-day-old WT and *Ospelo* plants. Scale bar = 0.5 mm. (G) Size of acetocarmine-stained root apical meristems of 4-day-old WT and *Ospelo* plants. Error bars represent the s.d. (n = 10) (H) Base, middle and tip regions of leaves from 30- and 60-day-old WT and *Ospelo* plants. Scale bars = 1 cm. (I) Trypan blue staining of leaves from 60-day-old WT and *Ospelo* plants Leaves decolorized directly by ethanol were included as control. Scale bars = 1 mm. The asterisks in (B), (E) and (G) indicate a significant difference between the WT and *Ospelo* ($P < 0.01$, by Student's t-test).

patterns and the quiescent centre (QC) of the stem cell niche in *Ospelo* were comparable with those of the WT (Fig. 1C). The cell length of maturation zones of *Ospelo* was also similar to that in the WT (Fig. 1C). To determine the root meristem activity of *Ospelo*, 4-day-old seedlings were cultured for 2 h in the presence of the thymidine analogue EdU, and *in situ* incorporation of EdU into DNA during active DNA synthesis in the root tip was visualized (Kotogány *et al.*, 2010). Compared with the WT, *Ospelo* had reduced levels of EdU labelling in the root meristem (Fig. 1D, E). Consistent with this, the traditional acetocarmine staining also showed that the meristematic region in *Ospelo* was reduced compared with the WT (Fig. 1F, G). Taken together, these results suggested that the meristematic activity in the *Ospelo* root is compromised.

Moreover, lesion-mimic spots appeared on *Ospelo* leaves after being grown in culture solution for about 20 d. The spotted-leaf phenotype became more severe as plants grew and expanded into whole leaves of 60-day-old *Ospelo* (Fig. 1H). In order to examine the occurrence of cell death or irreversible membrane damage, leaves of the WT and *Ospelo* were stained with trypan blue. As expected, there were clearly dyed blue spots on *Ospelo* leaves, while no detectable staining was observed on WT leaves (Fig. 1I).

Critical roles of OsPelo *in development and fertility*

The mature stage development and fertility of *Ospelo* were severely impaired (Fig. 2A, B). The plant height, tiller number and seed setting rate of *Ospelo* were all significantly decreased compared with the WT (Fig. 2C). However, the 1000-grain weight of *Ospelo* was similar to that of the WT (data not shown). To find the cause of the fertility defect, reproductive organs of *Ospelo* were further examined. There was no significant difference in pistils of *Ospelo* and the WT (Fig. 2D), and a successful cross using *Ospelo* as the female for the mapping population also confirmed its normal female fertility (data not shown). However, anthers of *Ospelo* were found to be pale compared with the healthy yellow anthers of the WT, indicating a severe defect in pollen development (Fig. 2E). Further staining analysis showed that pollen development of *Ospelo* was dysfunctional and their fertility was dramatically lower than in the WT (Fig. 2F).

Map-based cloning of OsPelo

To identify the mutated gene, an F_2 population was developed by crossing the *Ospelo* mutant with Nipponbare

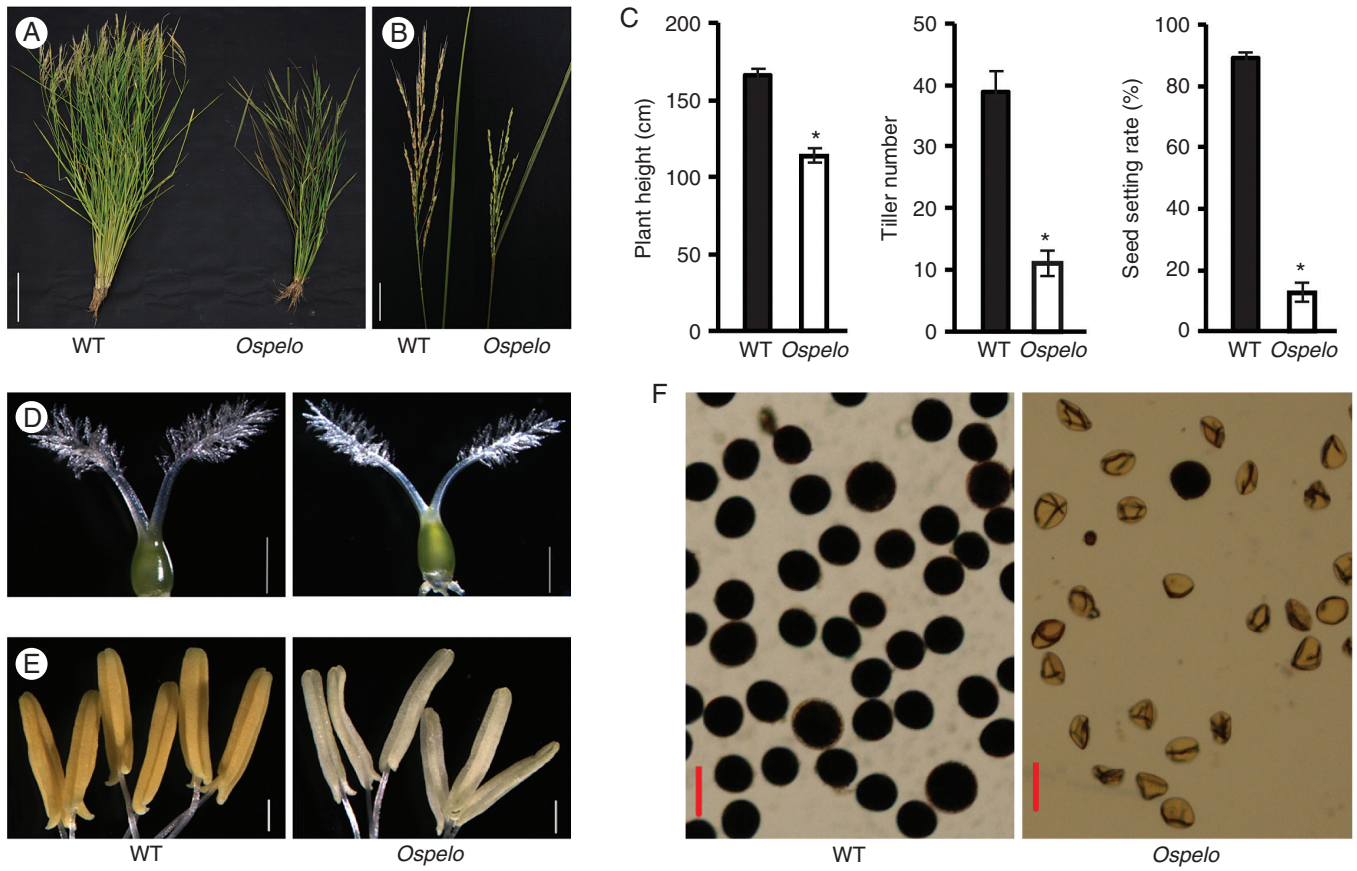

FIG. 2. Comparison of agronomic traits and reproductive organs in the WT and *Ospelo*. (A) Mature WT and *Ospelo* plants. Scale bar = 20 cm. (B) Spikes of the WT and *Ospelo*. Scale bar = 4 cm. (C) Plant height, tiller number and seed setting rate of the WT and *Ospelo* at the maturation stage. Error bars represent the s.d. (n = 20). (D) Pistils of the WT and *Ospelo*. Scale bars = 0.5 mm. (E) Stamens of the WT and *Ospelo*. Scale bars = 0.5 mm. (F) I_2–IK solution staining of pollen from the WT and *Ospelo*. Scale bars = 50 μm

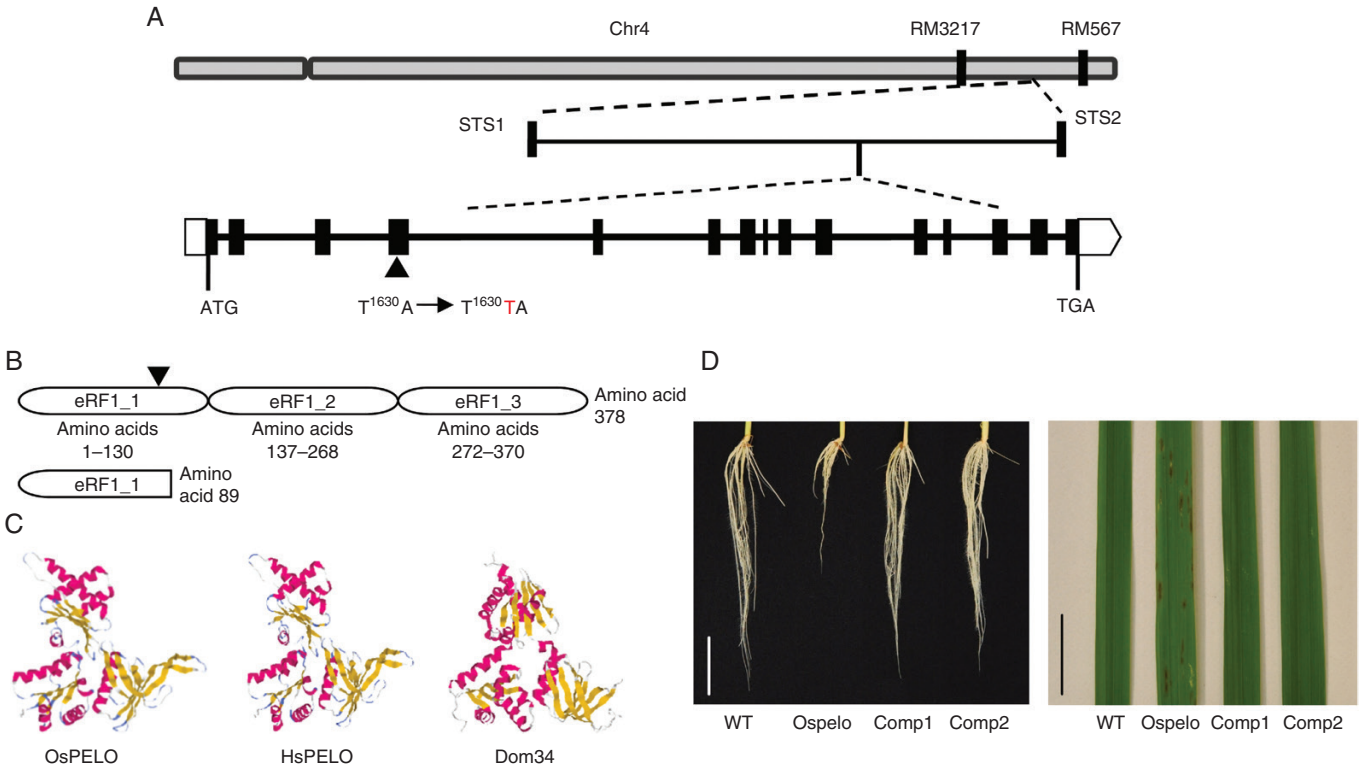

FIG. 3. *OsPelo* encodes the PELO protein in rice. (A) Map-based cloning of *OsPelo*. Black boxes represent exons, and lines represent introns. White boxes indicate untranslated regions. The arrowhead shows the site of the single-base insertion after the nucleotide 1630 bp downstream of ATG. (B) Predicted domains of OsPELO by the pfam database (pfam.xfam.org). The arrowhead indicates the insertion within the eRF1_1 domain, which results in the production of a truncated peptide with 89 amino acid residues. (C) The ribbon diagram of the 3-D structure of OsPELO predicted by SWISS-MODEL (https://swissmodel.expasy.org). The other two ribbon diagrams are published crystal structures of PELO from human (SWISS-MODEL Template Library ID: 5LZW.78) and Dom34 from yeast (PDB ID: 2VGM). (D) Complementation analysis of *Ospelo*. The root and leaf phenotype of O*spelo* was completely recovered by transformation of *OsPelo* driven by its native promoter. Two independent lines of transgenic plants (Comp1 and Comp2) in the O*spelo* mutant background are shown. Scale bar left = 4 cm; right = 1 cm.

(*japonica*). The F_1 seedlings displayed the WT phenotype and their F_2 progeny showed segregation of WT and *Ospelo* phenotypes at a ratio close to 3:1 (257:81, $\chi^2 = 0.32$, $P < 0.05$), indicating that the *Ospelo* phenotype was controlled by a single recessive nuclear gene. The *OsPelo* locus was first mapped to chromosome 4 between simple sequence repeat (SSR) markers RM3217 and RM567 using 30 F_2 mutant plants (Fig. 3A). The *OsPelo* gene was further mapped to a 411 kb region between two new STS markers STS1 and STS2 using 538 F_2 mutant plants (Fig. 3A). Fifty-two open reading frames (ORFs) were predicted in this region (http://rice.plantbiology.msu.edu/). Sanger sequencing analysis for both the WT and *Ospelo* mutant identified one single-base insertion after 1630 bp from the start codon on the fourth exon of LOC_Os04g56480 (Fig. 3A). The insertion introduced a premature stop codon and putatively yielded a peptide with 89 amino acid residues (Fig. 3B). LOC_Os04g56480 encodes rice Pelota, which is the homologue of Pelota in *Drosophila* (Eberhart and Wasserman, 1995). Therefore, we named it *OsPelo*. The *OsPelo* gene is 7945 bp in length, and contains 15 exons and 14 introns. The protein-coding region of *OsPelo* is 1137 bp and encodes a 378 amino acid protein. The protein structure is consistent with the annotation generated by pfam (pfam.xfam.org), with three conserved eRF1 domains (Fig. 3B). A search in the rice genome with the full-length OsPELO protein sequence using BLASTp showed that it is a single-copy gene.

PELO is a conserved protein involved in the mRNA NGD pathway based on its structural similarity to tRNA (Kobayashi *et al.*, 2010). The putative tertiary structure of OsPELO was predicted using the online SWISS-MODEL server (https://swissmodel.expasy.org) (Biasini *et al.*, 2014). As expected, its structure showed high similarity to those of human and yeast PELOs, with three conserved domains arranged in an L-shape (Fig. 3C). This further confirms that OsPELO is the rice homologue of PELO.

Functional complementation test of Ospelo

To confirm that the single nucleotide insertion in *OsPelo* is responsible for the mutant phenotype, complementation analysis was conducted using *A. tumefaciens*-mediated transformation. The protein-coding region of *OsPelo* was cloned into a binary vector driven by its 2264 bp native promoter and used for transformation of *Ospelo*. More than 20 independent transgenic lines were obtained. The short root and spotted-leaf phenotype was restored in all the positive transformants (Fig. 3D). These results demonstrate that the single base insertion in *OsPelo* causes the short root and spotted-leaf phenotype in *Ospelo*.

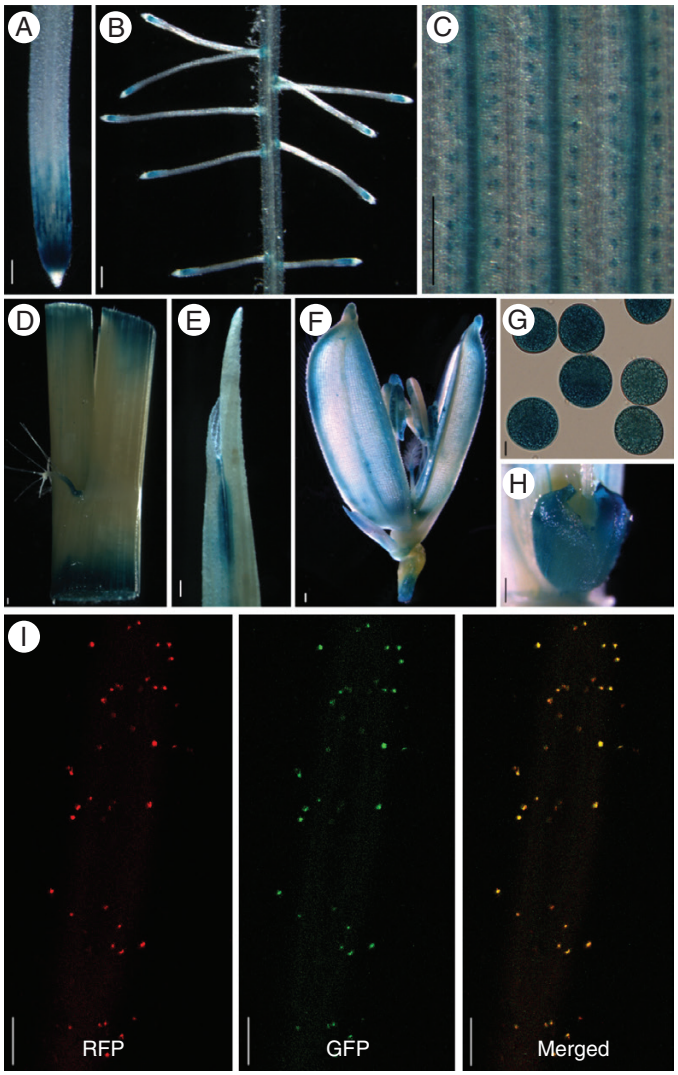

FIG. 4. Expression pattern of *OsPelo* and sub-cellular localization of OsPELO. (A–H) Histochemical staining analysis of expression of the *OsPelo* promoter–GUS fusion in various tissues. GUS signals were detected in the primary root tip (A), the tip and base of lateral roots (B), leaf vein and guard cells (C), stem and auricle (D), ligule (E), young spikelet (F), pollen (G) and paddle (H). Scale bars = 0.2 mm in (A–F, H), 10 μm in (G). (I) OsPELO targets GFP to mitochondria in transiently transformed onion epidermal cells. The AOX–RFP is used as the mitochondrial marker. Scale bars = 10 μm.

Expression pattern and sub-cellular localization analysis of OsPelo

To determine the tissue-specific expression pattern of *OsPelo*, a 2264 bp native promoter was fused to the GUS reporter gene. This chimeric gene cassette was used to transform WT plants via the *A. tumefaciens*-mediated transformation method. Histochemical staining for GUS activity in T_2 plants showed that *OsPelo* was ubiquitously expressed in plant organs, including the primary root tip, tip and base of lateral roots, leaf vein and guard cells, stem and auricle, ligule, lemma, anther, stigma, glume, peduncle, pollen and paddle (Fig. 4A–H).

Furthermore, online prediction tools were employed to predict the sub-cellular localization of OsPELO. A mitochondrial localization was suggested with a high probability by MitoProt II (https://ihg.gsf.de/ihg/mitoprot.html; Claros *et al.*, 1996) and WoLF PSORT (https://wolfpsort.hgc.jp; Horton *et al.*, 2007) and a lower probability by TargetP (http://www.cbs.dtu.dk/services/TargetP; Emanuelsson *et al.*, 2000). To examine the sub-cellular localization of OsPELO experimentally, a chimeric fusion gene of the coding region of *OsPelo* and GFP under the control of the 35S promoter was constructed and delivered into onion epidermal cells for transient expression. Fluorescence analysis showed that the fusion protein co-localized with a co-transformed mitochondrial marker (Fig. 4I), indicating that OsPELO is located in mitochondria.

Enhanced disease resistance in Ospelo

The occurrence of necrotic spots in *Ospelo* resembles the hypersensitive response (HR) after infection by pathogens. A number of spotted-leaf mutants showed enhanced resistance to bacterial and/or fungal pathogens (Fekih *et al.*, 2015; Wang *et al.*, 2017). To examine whether *Ospelo* also gains disease resistance, WT and *Ospelo* plants were inoculated with three races of *Xoo*, the causal agent of rice bacterial blight. The *Ospelo* plants exhibited significantly enhanced resistance to all tested *Xoo* strains (PXO71, PXO99 and PXO145) compared with the WT (Fig. 5A, B).

Defence response genes were commonly induced during lesion development in a number of rice spotted-leaf mutants (Fekih *et al.*, 2015; Wang *et al.*, 2015). Therefore, we detected expression of three pathogenesis-related (PR) marker genes (*PR1b*, *PR10* and *PO-C1*) associated with defence response. The results showed that all these PR marker genes were highly upregulated in *Ospelo* (Fig. 5C).

Whole-genome expression analysis of Ospelo

PELO is a conserved key member of the RNA surveillance pathway and known to be involved in ribosome rescue, spermatogenesis, cell cycle control and meiotic cell division. However, almost all this knowledgs was from studies in yeast and mammals, with little information in plants. To gain further insight into the *in planta* function of *OsPelo*, transcriptome sequencing analysis of WT and *Ospelo* plants was conducted using RNA sequencing (RNA-seq). As lesion-mimic spots started to emerge on 20-day-old *Ospelo* leaves, this stage was selected for the profiling analysis. Three replicates of each genotype were used, yielding six libraries in total. Each of these libraries generated >20 million 125 bp paired-end reads after quality control, and about 86 % of them were uniquely mapped onto the rice reference genome (Supplementary Data Table S2).

A total of 4990 DEGs were identified with a cut-off of the FDR-adjusted *P*-value <0.05. Among them, 2914 DEGs showed higher expression in *Ospelo* than in the WT, and were termed upregulated genes, while 2076 DEGs showed lower expression in *Ospelo* than in the WT and were termed downregulated genes (Fig. 6A; Supplementary Data Table S3). Among these DEGs, more than half of upregulated and downregulated genes showed a fold change <2 (Fig. 6B). This is in line with what

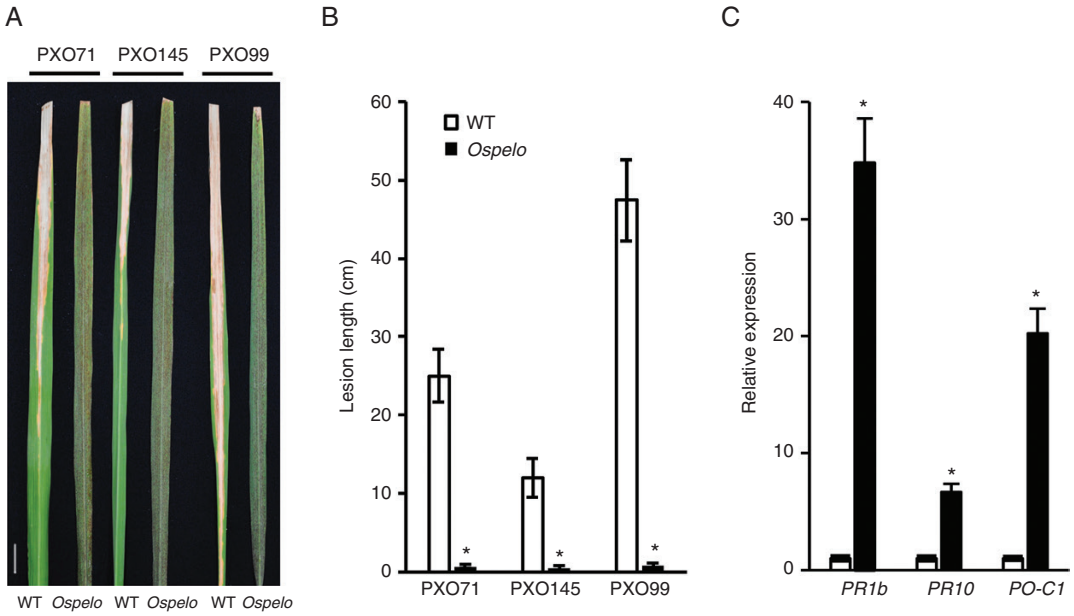

FIG. 5. Detection of bacterial blight pathogen resistance and expression of resistance-related genes. (A) Reactions of the WT and *Ospelo* to three *Xanthomonas oryzae* pv. *oryzae* (*Xoo*) isolates. Scale bar = 2 cm. (B) Lesion lengths of the WT and *Ospelo* produced by three *Xoo* isolates measured 3 weeks after infection. Data are means ± s.d. of ten plants. (C) Relative expression of pathogenesis-related genes. WT and *Ospelo* leaves were collected from seedlings at the tillering stage. Data are means ± s.d. of three biological replicates (Student's *t*-test: $*P < 0.01$).

was expected when considering that the leaf samples selected were at the very early stage of phenotypic change.

To analyse further the effects of *OsPelo* mutation on the transcriptomes, GO classification analysis of the up- and downregulated DEGs was conducted (Fig. 6C–E; Supplementary Data Table S4). Within the category of biological process, upregulated genes were largely associated with response to stress, secondary metabolic process and cell death, indicating that the stress response in *Ospelo* was activated (Fig. 6C). Genes involved in post-embryonic development, reproduction and embryo development were significantly enriched among downregulated genes, which was consistent with the defects in root development and fertility in *Ospelo*. Moreover, genes involved in translation, metabolic process, transport, photosynthesis and biosynthesis were also enriched in downregulated genes. Within the category of molecular function, genes involved in catalytic activity, kinase activity and oxygen binding activity were enriched among upregulated genes, while genes involved in transcription factor activity and RNA binding were specifically enriched among downregulated genes (Fig. 6D). In terms of cellular component, only the plasma membrane was significantly enriched among upregulated genes, while downregulated genes showed association with the plastid, mitochondrion, cytosol, nucleolus and cytoskeleton, suggesting a broad range of functional repression of organelles in *Ospelo* (Fig. 6E).

To explore further the biological pathways in which *OsPelo* may be involved, we performed KEGG pathway enrichment analysis for the DEGs between *Ospelo* and the WT. Twenty-three pathways were significantly enriched for upregulated genes and 53 for downregulated genes (Supplementary Data Table S5). Among the top 15 enriched pathways, the highly enriched upregulated pathways were mainly related to plant–pathogen interaction, protein processing, carbohydrate metabolism (amino sugar and nucleotide sugar metabolism, glycolysis/gluconeogenesis), amino acid metabolism (phenylalanine and glutathione metabolism), lipid metabolism (fatty acid metabolism, fatty acid elongation, biosynthesis of unsaturated fatty acids, α-linolenic acid metabolism, peroxisome) and secondary metabolism (biosynthesis of secondary metabolites, phenylpropanoid and flavonoid) (Fig. 7A). This was consistent with the enhanced pathogen resistance in *Ospelo* (Fig. 5A, B). The highly enriched pathways associated with down-regulated genes were mainly related to translation (aminoacyl-tRNA biosynthesis, RNA transport, ribosome biogenesis in eukaryotes), mismatch repair and primary metabolism including nucleotides, carbohydrates and amino acids (Fig. 7B).

In total, 30 DEGs were found to be involved in the aminoacyl-tRNA biosynthesis pathway, among which 28 DEGs responsible for synthesis of most aminoacyl-tRNAs were significantly downregulated in *Ospelo* (Fig. 7C; Supplementary Data Table S6). Further MapMan classification of DEGs also showed that a number of gene bins in the RNA–protein synthesis pathway were greatly downregulated, including RNA transcription and processing, protein amino acid activation, and protein synthesis initiation, elongation and release (Fig. 7D). These results were consistent with the putative role of *OsPelo* in stalled ribosome release in the mRNA decay pathway, whose dysfunction would result in the repression of translation.

Among the enriched KEGG pathways for upregulated genes, there were several biotic stress-related pathways, including plant–pathogen interaction, α-linolenic acid metabolism and phenylpropanoid biosynthesis (Fig. 7A). The α-linolenic acid metabolism pathway is responsible for jasmonic acid (JA) synthesis, and the phenylpropanoid biosynthesis pathway produces lignin. JA is one of major signalling pathways in plant disease resistance (Nahar *et al.*, 2011; Xie *et al.*, 2011). Lignin

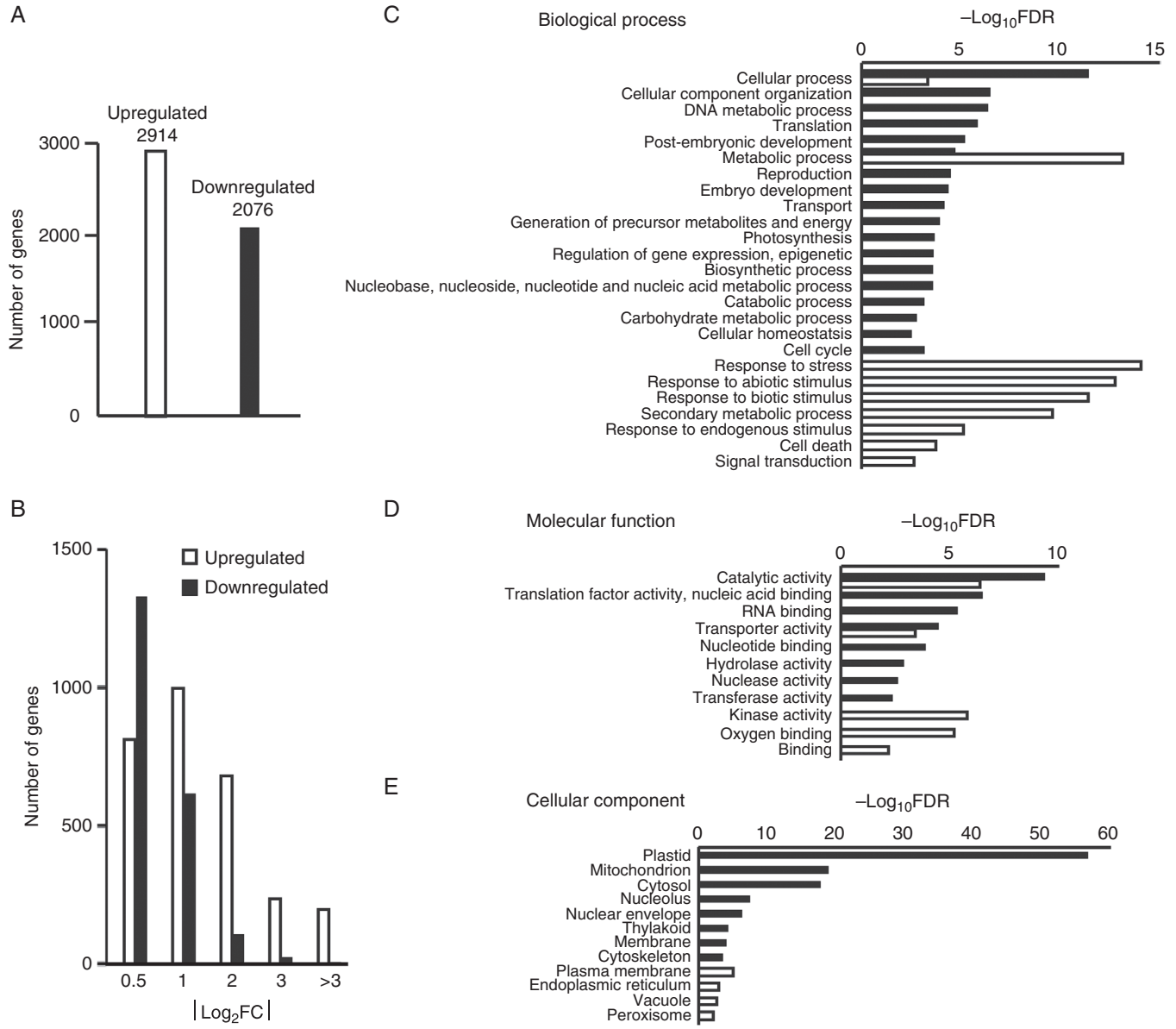

FIG. 6. Analysis and Gene Ontology (GO) enrichment of differentially expressed genes (DEGs) between the WT and *Ospelo* by RNA-seq. (A) The number of up- and downregulated DEGs between the WT and *Ospelo*. (B) The fold change distribution of DEGs between the WT and *Ospelo*. (C–E) GO term enrichment analysis of up- and downregulated DEGs in Biological process (C), Molecular function (D) and Cellular component (E).

is a non-degradable mechanical barrier for most micro-organisms, and an increase in lignification is a common response to pathogen attack to block parasite invasion and reduce the susceptibility of hosts (Moura *et al.*, 2010). Consistent with these findings, MapMan analysis clearly showed that the synthesis pathways for JA and lignin were both significantly activated (Fig. 7E, F).

DISCUSSION

In the present study, a rice mutant, *Ospelo*, was isolated from an EMS-mutagenized population of rice (*indica*, 'Kasalath'). The mutation caused loss of function of Pelota, a rice homologue of a key component in the NGD pathway. The mutant showed defects in root system development and spotted leaves from the early seedling stage, semi-dwarfness and defective pollen development (Figs 1 and 2). Functional complementation with WT *OsPelo* rescued the mutant phenotype observed in *Ospelo* (Fig. 3). We further conducted transcriptome sequencing of *Ospelo* and the WT, and found that DEGs were significantly associated with a number of biological processes, including translation, metabolism and biotic stress response.

OsPELO belongs to a family of evolutionarily conserved proteins called PELO, with their primary function in the regulation of translation and cell cycle progression. In *Drosophila*, *Pelo* has been shown to be required to control meiotic cell cycle progression and self-renewal and division of GSCs in the ovary (Eberhart and Wasserman, 1995; Xi *et al.*, 2005). The yeast

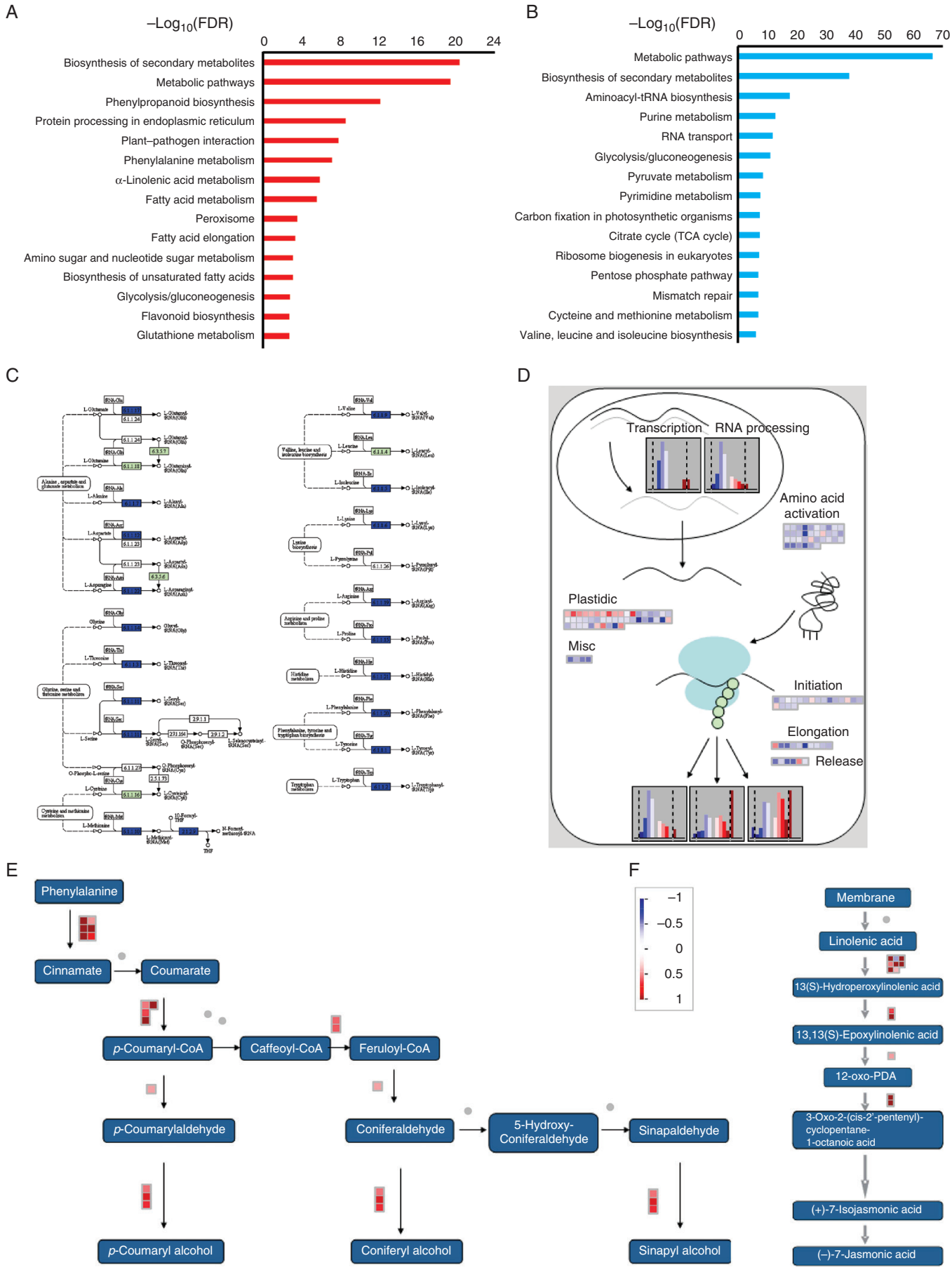

homologue of PELO, DOM34, functions in protein translation to promote G_1 progression and differentiation, and the *dom34* mutants grow slowly and have defects in meiosis and sporulation (Davis and Engebrecht, 1998). In mice, disruption of the *Pelo* gene results in early embryonic lethality and defects in cell cycle progression (Adham *et al.*, 2003). In rice *Ospelo* mutants, the root meristem activity was repressed, and pollen fertility and seed setting rate were dramatically decreased, suggesting a conserved role for *OsPelo* in cell cycle control through translation. Genes involved in translation, including aminoacyl-tRNA biosynthesis, protein amino acid initiation, elongation and release, were significantly enriched among the downregulated genes, suggesting the repression of translation in *Ospelo* (Fig. 7C, D; Supplementary Data Table S5). The mitochondrial localization of OsPELO suggests its possible involvement in the translation process taking place in mitochondria, one of the only two organelles containing their own genomes in cells (Fig. 4I). It has been reported that the PELO proteins are located in the cytoplasm of *Drosophila* (Xi *et al.*, 2005) and in the cytoskeleton of mammalian cells (Burnicka-Turek *et al.*, 2010). The difference in sub-cellular localization of PELO proteins among different species might suggest their functional divergence during evolution.

The cell cycle is controlled by a complex machinery composed of cyclins, cyclin-dependent kinases (CDKs), CDK inhibitors (CKIs), E2F transcription factors and a number of other proteins (Inzé and Veylder, 2006; Guo *et al.*, 2007). Among them, the A-type CDKs (CDKAs) are essential for G_1 to S and G_2 to M transition, and the B-type CDKs (CDKBs) show maximum activity at the G_2 to M transition and the M-phase (De Veylder *et al.*, 2007; Endo *et al.*, 2012). D-type cyclins (CYCDs) mainly regulate the G_1 to S transition through association with CDKs. In addition, the binding of CKI proteins could also adjust CDK activity (Polyn *et al.*, 2015). The overexpression of one *CKI* gene, *KRP1*, could result in reduced cell production during leaf development and seed filling, and disturbed production of endosperm cells (Barrôco *et al.*, 2006). Consistent with this, several key regulatory components of the cell cycle were found to be downregulated, including two cyclin genes (*CycD3;1* and *CycF2;3*), seven CDK genes (*CDKA;1*, *CDKB1;1*, *CDKB2;1*, *CDKD;1*, *CKL1*, *CKL6* and *CKL7*) and one E2F transcription factor gene (*E2F2*) (Supplementary Data Table S7). Moreover, *KRP1* was found to be upregulated. These data suggested that the cell cycle progression in *Ospelo* was repressed, which might explain the observed short root phenotype.

Defence response might be activated without pathogen attack in spotted-leaf mutants, and contribute to enhanced resistance to pathogen infection (Wang *et al.*, 2017). Recently PELO has been reported to be involved in general antiviral activity in *Drosophila* and resistance to begomovirus in tomato (Wu *et al.*, 2014; Lapidot *et al.*, 2015). Mutation or silencing of *Pelo* similarly resulted in virus resistance in both *Drosophila* and tomato, and the critical role of PELO in highly efficiently translating viral proteins of infective viruses was suggested. The loss-of-function *OsPelo* mutation results in HR-like lesion spots on leaves and enhanced resistance to bacterial blight (Fig. 5A, B). The expression of three PR marker genes, *PR1b*, *PR10* and *PO-C1*, was significantly upregulated in *Ospelo* during the development of lesion spots (Fig. 5C), indicating activation of PR genes and their possible roles in the enhanced pathogen resistance. Furthermore, whole-genome transcriptome analysis showed that there were 40 *PR* genes in the DEGs and all but one of them were significantly upregulated in *Ospelo* (Supplementary Data Table S8).

Salicylic acid (SA) and JA are two conserved positive regulators of defence response in plants and are proposed to activate a common pathogen defence system in rice (Tamaoki *et al.*, 2013; Berens *et al.*, 2017). SA-mediated redox status changes control the nucleocytoplasmic localization of NPR1, and it interacts with TGA transcription factors upon localization to the nucleus and activates SA-responsive genes encoding PR proteins (Dong, 2004; Koornneef and Pieterse, 2008). Analysis of DEGs in *Ospelo* identified seven SA biosynthesis-related *PAL* genes, two *NPR* genes (*NPR1* and *NPR4*), four TGA transcription factor genes, 20 JA biosynthesis-associated genes and three *JAZ* genes (Supplementary DataTable S9). All but three of them were upregulated in *Ospelo*, suggesting that *OsPelo* plays a negative role in both SA and JA biosynthesis and/or signalling and its loss of function might cause higher accumulation of SA and JA, thus enhancing plant defence against pathogens. Moreover, WRKY transcription factors are also proposed to be critical components in SA-dependent defence responses and control *PR* gene expression (Koornneef and Pieterse, 2008; Wei *et al.*, 2013). In our study, there were 37 *WRKY* genes showing differential expression in *Ospelo* compared with the WT, and 34 of them were upregulated (Supplementary Data Table S10). Among them there were a number of WRKYs which have been reported to regulate pathogen resistance in rice (Liu *et al.*, 2005; Chujo *et al.*, 2007; Qiu *et al.*, 2007; Shimono *et al.*, 2007; Peng *et al.*, 2008; Chujo *et al.*, 2013; Yokotani *et al.*, 2013).

The KEGG enrichment analysis indicated the constitutive activation of the plant–pathogen interaction pathway (Fig. 7A). A total of 41 genes in the pathway were found to be differentially expressed in *Ospelo* compared with the WT, and all of them except two *CNGC* genes were upregulated (Supplementary Data Table S11). These genes participated in pathogen-associated molecular patterning (PAMP)-triggered immunity (PTI) and effector-triggered immunity (ETI) pathways in innate immunity. Within the PTI pathway, there were two *CNGC* genes (*CNGC12* and *CNGC10*), one *CAM* gene (*Cam1-1*), 15 *CML* genes and four *CPK* genes (*CPK10*, *CPK20*, *CPK21* and *CPK23*) involved in calcium signalling; two *Rboh* genes (*Rboh5* and *Rboh7*) involved in generation of reactive oxygen species (ROS) and *NOS1* for nitric oxide production; and two *PR1* genes as antimicrobial components. Within the ETI pathway, *RIN4*, *RPS2*, *SGT1* and three *RPM1* genes were involved in recognition of avirulent effectors; and there were two *HSP90* genes for HR. The loss-of-function mutation of *CNGC* in arabidopsis and barley resulted in high levels of SA, constitutive expression of PR genes and enhanced resistance to pathogens (Clough *et al.*, 2000; Balagué *et al.*, 2003; Rostoks *et al.*, 2006; Kaplan *et al.*, 2007). Overexpression of *OsCPK10*

FIG. 7. Pathway enrichment and MapMan analysis of DEGs between the WT and *Ospelo*. (A, B) Kyoto Encyclopedia of Genes and Genomes (KEGG) pathway enrichment of up- (A) and downregulated (B) DEGs. (C) Mapping of DEGs associated with the KEGG aminoacyl-tRNA biosynthesis pathway. Boxes labelled with blue colour indicate downregulated DEGs between the WT and *Ospelo*. (D–F) MapMan analysis of DEGs associated with RNA–protein synthesis (D), lignin synthesis (E) and JA synthesis (F).

and *OsCPK20* in rice activated both SA- and JA-dependent defence responses and enhanced the resistance of transgenic plants to pathogens (Fu *et al*., 2013, 2014). These results showed that both the PTI- and ETI-related signalling components were significantly upregulated in *Ospelo*, suggesting that the loss of function of *OsPelo* resulted in activation of both PTI and ETI, reinforcement of cell walls and induction of PR proteins, thus enhancing resistance of *Ospelo* to pathogens.

In conclusion, we report herein that *OsPelo* functions in development and defence in rice. We characterized the roles of this rice homologue of PELO protein, and confirmed that loss of function of *OsPelo* resulted in defects in root system development and enhanced pathogen resistance in rice.

SUPPLEMENTARY DATA

Supplementary data are available online at https://academic.oup.com/aob and consist of the following. Table S1: primers used in the study. Table S2: RNA-seq output and mapping results. Table S3: differentially expressed genes (DEGs) between the WT and *Ospelo*. Table S4: GO enrichment analysis of DEGs. Table S5: KEGG pathway enrichment analysis of DEGs. Table S6: list of DEGs associated with aminoacyl-tRNA biosynthesis. Table S7: list of DEGs associated with cell cycle regulation. Table S8: list of 40 *PR* genes found in DEGs. Table S9: list of DEGs associated with SA and JA biosynthesis and signalling. Table S10: list of 37 *WRKY* genes found in DEGs. Table S11: list of 41 DEGs involved in plant–pathogen interaction.

ACKNOWLEDGEMENTS

This work was supported by the National Natural Science Foundation of China [grant nos 31371595 and 31300246], the Zhejiang Provincial Natural Science Foundation of China [grant nos LY17C020002 and LQ16C020001], the Natural Science Foundation of Ningbo [grant no. 2017A610291] and the K. C. Wong Magna Fund in Ningbo University.

LITERATURE CITED

Adham IM, **Sallam MA**, **Steding G**, ***et al.*** **2003**. Disruption of the pelota gene causes early embryonic lethality and defects in cell cycle progression. *Molecular and Cellular Biology* **23**: 1470–1476.

Anders S, **Pyl PT**, **Huber W. 2015**. HTSeq – a python framework to work with high-throughput sequencing data. *Bioinformatics* **31**: 166–169.

Balagué C, **Lin B**, **Alcon C**, ***et al.*** **2003**. HLM1, an essential signaling component in the hypersensitive response, is a member of the cyclic nucleotide-gated channel ion channel family. *The Plant Cell* **15**: 365–379.

Barrôco RM, **Peres A**, **Droual A-M**, ***et al.*** **2006**. The cyclin-dependent kinase inhibitor Orysa;KRP1 plays an important role in seed development of rice. *Plant Physiology* **142**: 1053–1064.

Becker T, **Armache J-P**, **Jarasch A**, ***et al.*** **2011**. Structure of the no-go mRNA decay complex Dom34–Hbs1 bound to a stalled 80S ribosome. *Nature Structural and Molecular Biology* **18**: 715–720.

Berens ML, **Berry HM**, **Mine A**, **Argueso CT**, **Tsuda K. 2017**. Evolution of hormone signaling networks in plant defense. *Annual Review of Phytopathology* **55**: 401–425.

Biasini M, **Bienert S**, **Waterhouse A**, ***et al.*** **2014**. Swiss-model: modelling protein tertiary and quaternary structure using evolutionary information. *Nucleic Acids Research* **42**: W252–W258.

Burnicka-Turek O, **Kata A**, **Buyandelger B**, ***et al.*** **2010**. Pelota interacts with HAX1, EIF3G and SRPX and the resulting protein complexes are associated with the actin cytoskeleton. *BMC Cell Biology* **11**: 28.

Caryl AP, **Lacroix I**, **Jones GH**, **Franklin FCH. 2000**. An arabidopsis homologue of the *Drosophila* meiotic gene pelota. *Sexual Plant Reproduction* **12**: 310–313.

Chen L, **Muhlrad D**, **Hauryliuk V**, ***et al.*** **2010**. Structure of the Dom34–Hbs1 complex and implications for no-go decay. *Nature Structural and Molecular Biology* **17**: 1233–1240.

Chen S, **Jin W**, **Wang M**, ***et al.*** **2003**. Distribution and characterization of over 1000 T-DNA tags in rice genome. *The Plant Journal* **36**: 105–113.

Chujo T, **Takai R**, **Akimoto-Tomiyama C**, ***et al.*** **2007**. Involvement of the elicitor-induced gene OsWRKY53 in the expression of defense-related genes in rice. *Biochimica et Biophysica Acta* **1769**: 497–505.

Chujo T, **Miyamoto K**, **Shimogawa T**, ***et al.*** **2013**. OsWRKY28, a PAMP-responsive transrepressor, negatively regulates innate immune responses in rice against rice blast fungus. *Plant Molecular Biology* **82**: 23–37.

Claros MG, **Vincens P. 1996**. Computational method to predict mitochondrially imported proteins and their targeting sequences. *European Journal of Biochemistry* **241**: 779–786.

Clough SJ, **Fengler KA**, **Yu I-c**, **Lippok B**, **Smith RK**, **Bent AF. 2000**. The arabidopsis dnd1 'defense, no death' gene encodes a mutated cyclic nucleotide-gated ion channel. *Proceedings of the National Academy of Sciences, USA* **97**: 9323–9328.

Cole SE, **LaRiviere FJ**, **Merrikh CN**, **Moore MJ. 2009**. A convergence of rRNA and mRNA quality control pathways revealed by mechanistic analysis of nonfunctional rRNA decay. *Molecular Cell* **34**: 440–450.

Davis L, **Engebrecht J. 1998**. Yeast dom34 mutants are defective in multiple developmental pathways and exhibit decreased levels of polyribosomes. *Genetics* **149**: 45–56.

De Veylder L, **Beeckman T**, **Inze D. 2007**. The ins and outs of the plant cell cycle. *Nature Reviews. Molecular Cell Biology* **8**: 655–665.

Ding W, **Lin L**, **Zhang B**, ***et al.*** **2015**. OsKASI, a β-ketoacyl-[acyl carrier protein] synthase I, is involved in root development in rice (*Oryza sativa* L.). *Planta* **242**: 203–213.

Doma MK, **Parker R. 2006**. Endonucleolytic cleavage of eukaryotic mRNAs with stalls in translation elongation. *Nature* **440**: 561–564.

Dong X. 2004. NPR1, all things considered. *Current Opinion in Plant Biology* **7**: 547–552.

Eberhart CG, **Wasserman SA. 1995**. The *pelota* locus encodes a protein required for meiotic cell division: an analysis of G2/M arrest in *Drosophila* spermatogenesis. *Development* **121**: 3477–3486.

Elkenani M, **Nyamsuren G**, **Raju P**, ***et al.*** **2016**. Pelota regulates epidermal differentiation by modulating BMP and PI3K/AKT signaling pathways. *Journal of Investigative Dermatology* **136**: 1664–1671.

van den Elzen AMG, **Schuller A**, **Green R**, **Séraphin B. 2014**. Dom34–Hbs1 mediated dissociation of inactive 80S ribosomes promotes restart of translation after stress. *EMBO Journal* **33**: 265–276

Emanuelsson O, **Nielsen H**, **Brunak S**, **von Heijne G. 2000**. Predicting subcellular localization of proteins based on their n-terminal amino acid sequence. *Journal of Molecular Biology* **300**: 1005–1016.

Endo M, **Nakayama S**, **Umeda-Hara C**, ***et al.*** **2012**. CDKB2 is involved in mitosis and DNA damage response in rice. *The Plant Journal* **69**: 967–977.

Fekih R, **Tamiru M**, **Kanzaki H**, ***et al.*** **2015**. The rice (*Oryza sativa* L.) LESION MIMIC RESEMBLING, which encodes an AAA-type ATPase, is implicated in defense response. *Molecular Genetics and Genomics* **290**: 611–622.

Fu L, **Yu X**, **An C. 2013**. Overexpression of constitutively active *OsCPK10* increases *Arabidopsis* resistance against *Pseudomonas syringae* pv. *tomato* and rice resistance against *Magnaporthe grisea*. *Plant Physiology and Biochemistry* **73**: 202–210.

Fu LW, **Yu XC**, **An CC. 2014**. *OsCPK20* positively regulates *Arabidopsis* resistance against *Pseudomonas syringae* pv. *tomato* and rice resistance against *Magnaporthe grisea*. *Acta Physiologiae Plantarum* **36**: 273–282.

Guo J, **Song J**, **Wang F**, **Zhang XS. 2007**. Genome-wide identification and expression analysis of rice cell cycle genes. *Plant Molecular Biology* **64**: 349–360.

Guydosh Nicholas R, **Green R. 2014**. Dom34 rescues ribosomes in 3′ untranslated regions. *Cell* **156**: 950–962.

Hashimoto Y, **Takahashi M**, **Sakota E**, **Nakamura Y. 2017**. Nonstop-mRNA decay machinery is involved in the clearance of mRNA 5'-fragments produced by RNAi and NMD in *Drosophila melanogaster* cells. *Biochemical and Biophysical Research Communications* **484**: 1–7.

Horton P, **Park KJ**, **Obayashi T**, ***et al.*** **2007**. WoLF PSORT: protein localization predictor. *Nucleic Acids Research* **35**: W585–W587.

Ikeuchi K, **Yazaki E**, **Kudo K**, **Inada T. 2016**. Conserved functions of human Pelota in mRNA quality control of nonstop mRNA. *FEBS Letters* **590**: 3254–63.

Inzé D, **Veylder LD. 2006**. Cell cycle regulation in plant development. *Annual Review of Genetics* **40**: 77–105.

Ishimura R, **Nagy G**, **Dotu I**, ***et al.* 2014**. Ribosome stalling induced by mutation of a CNS-specific tRNA causes neurodegeneration. *Science* **345**: 455–459.

Kaplan B, **Sherman T**, **Fromm H. 2007**. Cyclic nucleotide-gated channels in plants. *FEBS Letters* **581**: 2237–2246.

Kauffman HE, **Reddy APK**, **Hsieh SPY**, **Merca SD. 1973**. An improved technique for evaluating resistance of rice varieties to *Xanthomonas oryzae*. *Plant Disease Reporter* **57**: 537–541.

Kirmizitas A, **Gillis WQ**, **Zhu H**, **Thomsen GH. 2014**. Gtpbp2 is required for BMP signaling and mesoderm patterning in *Xenopus* embryos. *Developmental Biology* **392**: 358–367.

Kobayashi K, **Kikuno I**, **Kuroha K**, ***et al.* 2010**. Structural basis for mRNA surveillance by archaeal Pelota and GTP-bound EF1α complex. *Proceedings of the National Academy of Sciences, USA* **107**: 17575–19579.

Koornneef A, **Pieterse CMJ. 2008**. Cross talk in defense signaling. *Plant Physiology* **146**: 839–844.

Kotogány E, **Dudits D**, **Horváth GV**, **Ayaydin F. 2010**. A rapid and robust assay for detection of S-phase cell cycle progression in plant cells and tissues by using ethynyl deoxyuridine. *Plant Methods* **6**: 5. doi: 10.1186/1746-4811-6-5.

Lapidot M, **Karniel U**, **Gelbart D**, ***et al.* 2015**. A novel route controlling begomovirus resistance by the messenger RNA surveillance factor Pelota. *PLoS Genet* **11**: e1005538. doi: 10.1371/journal.pgen.1005538.

Liu XQ, **Bai XQ**, **Qian Q**, **Wang XJ**, **Chen MS**, **Chu CC. 2005**. OsWRKY03, a rice transcriptional activator that functions in defense signaling pathway upstream of OsNPR1. *Cell Research* **15**: 593–603.

Love MI, **Huber W**, **Anders S. 2014**. Moderated estimation of fold change and dispersion for RNA-seq data with DESeq2. *Genome Biology* **15**: 550.

Moura JCMS, **Bonine CAV**, **De Oliveira Fernandes Viana J**, **Dornelas MC**, **Mazzafera P. 2010**. Abiotic and biotic stresses and changes in the lignin content and composition in plants. *Journal of Integrative Plant Biology* **52**: 360–376.

Nahar K, **Kyndt T**, **De Vleesschauwer D**, **Höfte M**, **Gheysen G. 2011**. The jasmonate pathway is a key player in systemically induced defense against root knot nematodes in rice. *Plant Physiology* **157**: 305–316.

Nyamsuren G, **Kata A**, **Xu X**, ***et al.* 2014**. Pelota regulates the development of extraembryonic endoderm through activation of bone morphogenetic protein (BMP) signaling. *Stem Cell Research* **13**: 61–74.

Pedersen K, **Canals F**, **Prat A**, **Tabernero J**, **Arribas J. 2014**. PELO negatively regulates HER receptor signalling and metastasis. *Oncogene* **33**: 1190–7.

Peng Y, **Bartley LE**, **Chen XW**, ***et al.* 2008**. OsWRKY62 is a negative regulator of basal and Xa21-mediated defense against *Xanthomonas oryzae* pv. *oryzae* in rice. *Molecular Plant* **1**: 446–458.

Polyn S, **Willems A**, **De Veylder L. 2015**. Cell cycle entry, maintenance, and exit during plant development. *Current Opinion in Plant Biology* **23**: 1–7.

Qiu DY, **Xiao J**, **Ding XH**, ***et al.* 2007**. OsWRKY13 mediates rice disease resistance by regulating defense-related genes in salicylate- and jasmonate-dependent signaling. *Molecular Plant-Microbe Interactions* **20**: 492–499.

Ragan MA, **Logsdon JM Jr**, **Sensen CW**, **Charlebois RL**, **Doolittle WF. 1996**. An archaebacterial homolog of pelota, a meiotic cell division protein in eukaryotes. *FEMS Microbiology Letters* **144**: 151–155.

Raju P, **Nyamsuren G**, **Elkenani M**, ***et al.* 2015**. Pelota mediates gonocyte maturation and maintenance of spermatogonial stem cells in mouse testes. *Reproduction* **149**: 213–21.

Rostoks N, **Schmierer D**, **Mudie S**, ***et al.* 2006**. Barley necrotic locus nec1 encodes the cyclic nucleotide-gated ion channel 4 homologous to the Arabidopsis HLM1. *Molecular and Genetic Genomics* **275**: 159–168.

Saito S, **Hosoda N**, **Hoshino S. 2013**. The Hbs1–dom34 protein complex functions in non-stop mRNA decay in mammalian cells. *Journal of Biological Chemistry* **288**: 17832–43.

Shamsadin R, **Adham IM**, **von Beust G**, **Engel W. 2000**. Molecular cloning, expression and chromosome location of the human pelota gene PELO. *Cytogenetics and Cell Genetics* **90**: 75–78.

Shamsadin R, **Adham IM**, **Engel W. 2002**.Mouse pelota gene (Pelo): cDNA cloning, genomic structure, and chromosomal localization. *Cytogenetic Genome Research* **97**: 95–99.

Shimono M, **Sugano S**, **Nakayama A**, ***et al.* 2007**. Rice WRKY45 plays a crucial role in benzothiadiazole-inducible blast resistance. *The Plant Cell* **19**: 2064–2076.

Shoemaker CJ, **Green R. 2011**. Kinetic analysis reveals the ordered coupling of translation termination and ribosome recycling in yeast. *Proceedings of the National Academy of Sciences, USA* **108**: E1392–E1398.

Shoemaker CJ, **Eyler DE**, **Green R. 2010**. Dom34:Hbs1 promotes subunit dissociation and peptidyl-tRNA drop-off to initiate no-go decay. *Science* **330**: 369–372.

Tamaoki D, **Seo S**, **Yamada S**, ***et al.* 2013**. Jasmonic acid and salicylic acid activate a common defense system in rice. *Plant Signaling and Behavior* **8**: e24260. doi: 10.4161/psb.24260.

Thimm O, **Bläsing O**, **Gibon Y**, ***et al.* 2004**. Mapman: a user-driven tool to display genomics data sets onto diagrams of metabolic pathways and other biological processes. *The Plant Journal* **37**: 914–939.

Trapnell C, **Roberts A**, **Goff L**, ***et al.* 2012**. Differential gene and transcript expression analysis of RNA-seq experiments with tophat and cufflinks. *Nature Protocols* **7**: 562–578.

Tsuboi T, **Kuroha K**, **Kudo K**, ***et al.* 2012**. Dom34:Hbs1 plays a general role in quality-control systems by dissociation of a stalled ribosome at the 3' end of aberrant mRNA. *Molecular Cell* **46**: 518–529.

Wang SH, **Lim JH**, **Kim SS**, ***et al.* 2015**. Mutation of *SPOTTED LEAF3* (*SPL3*) impairs abscisic acid-responsive signalling and delays leaf senescence in rice. *Journal of Experimental Botany* **66**: 7045–7059.

Wang S, **Lei C**, **Wang J**, ***et al.* 2017**. *SPL33*, encoding an eEF1A-like protein, negatively regulates cell death and defense responses in rice. *Journal of Experimental Botany* **68**: 899–913.

Wei T, **Ou B**, **Li J**, ***et al.* 2013**. Transcriptional profiling of rice early response to *Magnaporthe oryzae* identified OsWRKYs as important regulators in rice blast resistance. *PLoS One* **8**: e59720. doi: 10.1371/journal.pone.0059720.

Wu X, **He WT**, **Tian S**, ***et al.* 2014**. *pelo* is required for high efficiency viral replication. *PLoS Pathogens* **10**: e1004034. doi: 10.1371/journal.ppat.1004034.

Xi R, **Doan C**, **Liu D**, **Xie T. 2005**. Pelota controls self-renewal of germline stem cells by repressing a Bam-independent differentiation pathway. *Development* **132**: 5365–5374.

Xie XZ, **Xue YJ**, **Zhou JJ**, **Zhang B**, **Chang H**, **Takano M. 2011**. Phytochromes regulate SA and JA signaling pathways in rice and are required for developmentally controlled resistance to *Magnaporthe grisea*. *Molecular Plant* **4**: 688–696.

Yang F, **Zhao R**, **Fang X**, ***et al.* 2015**. The RNA surveillance complex Pelo–Hbs1 is required for transposon silencing in the *Drosophila* germline. *EMBO Reports* **16**: 965–974.

Yi X, **Du Z**, **Su Z. 2013**. PlantGSEA: a gene set enrichment analysis toolkit for plant community. *Nucleic Acids Research* **41**: W98–W103.

Yin Z, **Chen J**, **Zeng L**, ***et al.* 2000**. Characterizing rice lesion mimic mutants and identifying a mutant with broad-spectrum resistance to rice blast and bacterial blight. *Molecular Plant-Microbe Interactions* **13**: 869–876.

Yokotani N, **Sato Y**, **Tanabe S**, ***et al.* 2013**. WRKY76 is a rice transcriptional repressor playing opposite roles in blast disease resistance and cold stress tolerance. *Journal of Experimental Botany* **64**: 5085–5097.

Zhu ZX, **Liu Y**, **Liu SJ**, **Mao CZ**, **Wu YR**, **Wu P. 2012**. A gain-of-function mutation in *OsIAA11* affects lateral root development in rice. *Molecular Plant* **5**: 154–161.